

CALIBRATION OF A PMD-CAMERA USING A PLANAR CALIBRATION PATTERN TOGETHER WITH A MULTI-CAMERA SETUP

Ingo Schiller, Christian Beder and Reinhard Koch

Computer Science Department, Kiel University, Germany
{ischiller,beder,rk}@mip.informatik.uni-kiel.de

Commission III/1

KEY WORDS: Close Range Photogrammetry, 3D Sensors, Computer Vision, Calibration, Industrial Measurement, Adjustment, Fusion, Accuracy Analysis

ABSTRACT:

We discuss the joint calibration of novel 3D range cameras based on the time-of-flight principle with the Photonic Mixing Device (PMD) and standard 2D CCD cameras. Due to the small field-of-view (fov) and low pixel resolution, PMD-cameras are difficult to calibrate with traditional calibration methods. In addition, the 3D range data contains systematic errors that need to be compensated. Therefore, a calibration method is developed that can estimate full intrinsic calibration of the PMD-camera including optical lens distortions and systematic range errors, and is able to calibrate the external orientation together with multiple 2D cameras that are rigidly coupled to the PMD-camera. The calibration approach is based on a planar checkerboard pattern as calibration reference, viewed from multiple angles and distances. By combining the PMD-camera with standard CCD-cameras the internal camera parameters can be estimated more precisely and the limitations of the small fov can be overcome. Furthermore we use the additional cameras to calibrate the systematic depth measurement error of the PMD-camera. We show that the correlation between rotation and translation estimation is significantly reduced with our method.

1 INTRODUCTION

An important and fundamental requirement for many computer vision applications is the availability of 3D-range measurements. A standard method is the usage of a stereo-system consisting of two rigidly coupled standard CCD-cameras. However for real-time applications efficient dense real-time stereo algorithms are needed. These algorithms consume a significant amount of CPU and/or GPU resources, and might have problems in un-textured scenes. Within the last couple of years a new generation of active cameras has been developed based on the time-of-flight principle. These so called PMD-(Photonic Mixing Device) cameras (Lange et al., 1999),(Xu et al., 1998) emit modulated infrared (IR) light using LEDs with 20 MHz modulation frequency, and measure the time between emitting the modulated light and receiving the echo of the light using a special PMD correlation sensor element. This new technique delivers dense depth maps at a resolution up to 176x144 pixels at frame rates up to 25Hz. The cameras are suitable for near range measurements of up to 7.5 m distance and potentially offer dense depth at no additional computational costs (Kraft et al., 2004).

The cameras offer both a range image with pixel-wise depth and a reflectance image with IR modulation intensities. Due to the measurement with active illumination, the emitted light is concentrated to a small field-of-view (fov), typically around 20 degree horizontal fov. The resulting images are quite noisy and of low resolution. To overcome this shortcomings we propose to combine a PMD image with one or more high resolution CCD images. In this paper we address the exact calibration of such a PMD-camera in combination with at least one standard CCD-camera.

The combination of PMD-cameras with other measurement devices like standard CCD-cameras is gaining more importance as the advantages of the absolute range measurement of the PMD-camera and the higher resolution of the CCD-camera can be combined. The accuracy of stereo systems and PMD-cameras was

compared in (Beder et al., 2007a) and a fused surface reconstruction was proposed in (Beder et al., 2007b), which requires a reliable relative calibration of the stereo and the PMD camera. In (Kuhnert and Stommel, 2006) a fusion of PMD and stereo was proposed, where the accuracy of the results is highly dependent on the quality of the calibration. The relative orientation of a PMD and an optical camera for pose estimation is also required in (Prusak et al., 2007) and (Streckel et al., 2007).



Figure 1: The PMD-camera and additional CCD-cameras used for calibration.

Previous approaches to calibrate PMD cameras were described in (Kahlmann et al., 2006) and (Lindner and Kolb, 2006), who both use the calibration method of (Zhang, 1999) and (Bouguet, 1999) on the reflectance images to estimate internal and external orientation. The depth image is not used for pose estimation, because the scope of those works also is the depth calibration of the cameras. The authors conclude that the poor quality of the low resolution reflectance images makes precise localization very difficult (cf. also (Prasad et al., 2006), (Fuchs and May, 2007)).

We will present a novel approach for calibrating focal length, principle point, lens distortion and depth calibration for PMD-

and standard cameras in a joint method. Simultaneously we estimate the relative external transformation between the PMD- and CCD-cameras and achieve high accuracy by using multiple images from each camera. Our method uses the reflectance- and depth images provided by a PMD-camera and the reflectance images from the standard CCD-cameras. We use an analysis-by-synthesis approach, in combination with non-linear optimization for parameter estimation.

Section 2 introduces the geometric camera model and the depth calibration model. These models are used in section 3 to estimate the internal and external camera parameters using all images taken of a planar checkerboard calibration pattern. Finally we will present our results in section 4.

2 CAMERA CALIBRATION

In the calibration process we are estimating the internal camera parameters for the single cameras as well as the external parameters. We typically use 30 to 80 images per camera in the camera rig. So with four cameras we use up to 320 images in the calibration process. We assume a rigidly coupled camera rig and as a result we only estimate the absolute external camera parameters of the first camera in the rig. The positions and rotations of the other cameras are estimated relatively to this first camera. E.g. with four cameras and 20 images per camera we estimate 20 absolute external camera parameters (20x translation and rotation) and three (3x translation and rotation) relative external camera parameters.

The cameras will from now on carry the indexes $k, k \in (1, \dots, K)$, the images per camera will be indexed with indexes $j, j \in (1, \dots, M)$ and a pixel in an image is indexed with $i, i \in (1, \dots, N)$.

The initial estimation of the external orientations and internal parameters is based on correspondences between a reference object (here a planar checkerboard pattern) and points in the camera reflectance images. The detection of the checkerboard is done automatically if possible, otherwise the corners of the checkerboard have to be selected manually. Assuming that the checkerboard is located at the $Z = 0$ plane 2d-3d point correspondences can be established and the computation of the initial internal and external camera parameters is done using standard computer vision methods from OpenCV (Intel, n.d.).

2.1 Camera and Estimation Model

The geometric camera model assumed follows the definition in (Mugnier et al., 2004, p.229) and is defined as follows. A 3d point X_i is projected to a 2d point x_{ijk} according to the homogeneous equation:

$$\mathbf{x}_{ijk} \propto \mathbf{K}_k \mathbf{R}_{jk} (\mathbf{X}_i - \mathbf{C}_{jk}) \quad (1)$$

where \mathbf{C}_{jk} is the position of the j th image of the k th camera and \mathbf{R}_{jk} is the rotation of the j th image of the k th camera. x_{ijk} is the i th pixel in the j th image of the k th camera. The internal camera parameters are contained in the calibration matrix:

$$\mathbf{K}_k = \begin{pmatrix} f_{k,x} & s_k & x_{k,H} + \Delta x(\mathbf{x}_{ijk}, \mathbf{q}_k) \\ 0 & f_{k,y} & y_{k,H} + \Delta y(\mathbf{x}_{ijk}, \mathbf{q}_k) \\ 0 & 0 & 1 \end{pmatrix} \quad (2)$$

Note that we have one calibration matrix \mathbf{K}_k per camera. The additional factor $\Delta x(\mathbf{x}_{ijk}, \mathbf{q}_k)$ models the nonlinear lens distortion. The lens distortion is modeled following the definition

in (Heikkila and Silven, 1997) and has the parameters $\mathbf{q}_k = (r_1, r_2, t_1, t_2)$. From the initial camera parameter computation we have an estimate for principal point $(x_{k,H}, y_{k,H})$, shear s_k , focal lengths $(f_{k,x}, f_{k,y})$ and nonlinear distortion parameters. For the PMD-camera we also have depth images given, so that for each pixel \mathbf{x}_{ijk} in a PMD-image the corresponding depth $\lambda_{ijk}(d_l)$ is known. Note that the depth $\lambda_{ijk}(d_l)$ is dependent on the depth deviation parameters $d_l, l \in (0, \dots, 5)$ (see section 2.2). Hence, for each pixel the corresponding 3d point \mathbf{X}_i can be computed as follows:

$$\mathbf{X}_i = \lambda_{ijk}(d_l) \frac{\mathbf{R}_{jk}^T \mathbf{K}_k^{-1} \mathbf{x}_{ijk}}{\sqrt{\mathbf{x}_{ijk}^T \mathbf{K}_k^{-T} \mathbf{K}_k^{-1} \mathbf{x}_{ijk}}} + \mathbf{C}_{jk} \quad (3)$$

Assuming the planar calibration object to be located at the $Z = 0$ plane, one can derive one constraint per pixel by requiring $X_z = 0$ (X_z is the z -component of \mathbf{X}_i). Using equation (3) this is expressible as

$$\lambda_{ijk}(d_l) \mathbf{r}_{z,jk}^T \mathbf{K}_k^{-1} \mathbf{x}_{ijk} + C_{z,jk} \sqrt{\mathbf{x}_{ijk}^T \mathbf{K}_k^{-T} \mathbf{K}_k^{-1} \mathbf{x}_{ijk}} = 0 \quad (4)$$

or equivalent

$$\lambda_{ijk}(d_l) = - \frac{C_{z,jk} \sqrt{\mathbf{x}_{ijk}^T \mathbf{K}_k^{-T} \mathbf{K}_k^{-1} \mathbf{x}_{ijk}}}{\mathbf{r}_{z,jk}^T \mathbf{K}_k^{-1} \mathbf{x}_{ijk}} = f_{ijk}^{(1)} \quad (5)$$

where $\mathbf{r}_{z,jk} = (r_x, r_y, r_z)^T$ (the last column of the rotation matrix \mathbf{R}_{jk}) and $C_{z,jk} = z$ -component of \mathbf{C}_{jk} .

The depth constraint using only the planar reference object is obviously not sufficient for calibration. Hence the reflectance image has to be used as well. The second constraint that can be derived is, that the reflectance is assumed to be equal to the known reflectance of the reference object

$$I_{ref}(\mathbf{X}_i) = I_{ref} \left(\lambda_{ijk}(d_l) \frac{\mathbf{R}_{jk}^T \mathbf{K}_k^{-1} \mathbf{x}_{ijk}}{\sqrt{\mathbf{x}_{ijk}^T \mathbf{K}_k^{-T} \mathbf{K}_k^{-1} \mathbf{x}_{ijk}}} + \mathbf{C}_{jk} \right) = I(\mathbf{x}_{ijk}) \quad (6)$$

or by substituting $\lambda_{ijk}(d_l)$

$$I(\mathbf{x}_{ijk}) = I_{ref} \left(\mathbf{C}_{jk} - \frac{C_z \mathbf{R}_{jk}^T \mathbf{K}_k^{-1} \mathbf{x}_{ijk}}{\mathbf{r}_z^T \mathbf{K}_k^{-1} \mathbf{x}_{ijk}} \right) = f_{ijk}^{(2)} \quad (7)$$

where $I(\mathbf{x}_{ijk})$ denotes the reflectance image and I_{ref} denotes the reference image (here the image of a smoothed checkerboard pattern).

For the PMD-camera we can use both constraints (5) and (7) to estimate the external orientation and internal camera parameters. In the case of the standard CCD-cameras only the constraint (7) can be used. We will now show how to use these constraints to precisely calibrate the external and internal camera parameters as well as the depth calibration of the PMD-camera in a joint approach.

Figure 2 shows two input images to the calibration procedure from a PMD-camera. On the left the depth measurement and on the right a reflectance image is shown.

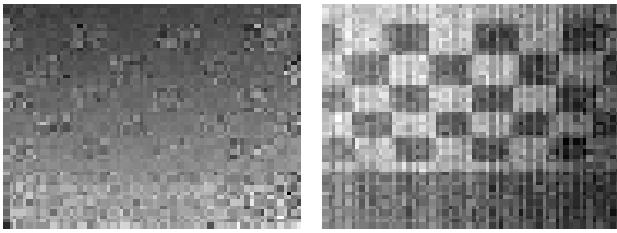


Figure 2: Depth image and grey value image from PMD-camera

2.2 Depth Calibration Model

The depth measurement with PMD-cameras suffers from systematic errors (Fuchs and May, 2007). The error is not only a constant offset but a higher order function (Kolb and Lindner, 2006). We chose to model the corrected depth as:

$$\lambda^* = d_0 + (1.0 + d_1) * \lambda + d_2 * x + d_3 * y + d_4 * \lambda^2 + d_5 * \lambda^3 \quad (8)$$

where λ^* is the corrected depth, x, y are the image coordinates, λ is the measured depth and $d_i, i \in (0, \dots, 5)$ are the parameters to estimate.

The depth deviation is dependent on the distance to the object and can be modeled as a polynomial because the modulation of the light is not perfectly sinusoidal. The factors d_2 and d_3 define a tilt in the image plane of the PMD-camera with respect to the optical axis, which was observed in the measurement data.

3 OPTIMIZATION

Now we will show, how the internal camera parameters and the external orientation can be determined from the depth and the reflectance image. From our estimate of the internal and external camera parameters we approximately know the internal camera parameters as well as rotation $R_{jk}^{(0)}$ and position $C_{jk}^{(0)}$ of our cameras. We will now show how to estimate those quantities starting from approximate initial values.

The rotation matrix can be represented using its Taylor expansion: (cf. (Förstner and Wrobel, 2004, p.53))

$$R_{jk}^{(\nu+1)} \approx R_{jk}^{(\nu)} + \begin{pmatrix} 0 & -\kappa & \phi \\ \kappa & 0 & -\omega \\ -\phi & \omega & 0 \end{pmatrix} \quad (9)$$

For every optimization step the relevant parameters are collected in a parameter vector \mathbf{p} . One can synthesize the depth image from the parameters using equation (5) as

$$\lambda_{ijk}(d_l) = f_{ijk}^{(1)}(\mathbf{p}) \approx f_{ijk}^{(1)}(\mathbf{p}^{(\nu)}) + \left. \frac{\partial f_{ijk}^{(1)}}{\partial \mathbf{p}} \right|_{\mathbf{p}^{(\nu)}} \Delta \mathbf{p} \quad (10)$$

and synthesize the reflectance image from the parameters using equation (7) as

$$I(\mathbf{x}_{ijk}) = f_{ijk}^{(2)}(\mathbf{p}) \approx f_{ijk}^{(2)}(\mathbf{p}^{(\nu)}) + \left. \frac{\partial f_{ijk}^{(2)}}{\partial \mathbf{p}} \right|_{\mathbf{p}^{(\nu)}} \Delta \mathbf{p} \quad (11)$$

Note, that in this formulation no derivative of any observed noisy low-resolution depth or reflectance image is required for the Taylor expansion. An efficient way to synthesize depth and reflectance image is to render the checkerboard on the GPU. We are exploiting this possibility here as we render checkerboard- and depth

image on the GPU including the full camera model. This significantly speeds up the calibration process.

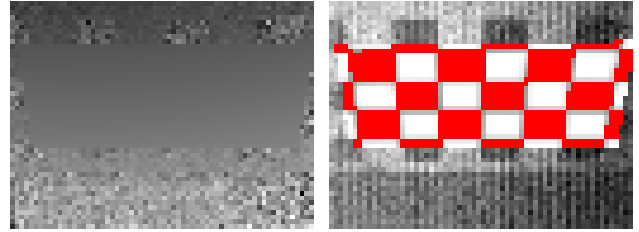


Figure 3: Depth image and grey value image from PMD-camera with reprojected checkerboard and depth plane

Figure 3 shows the synthesized images generated with equations 5 and 7. On the left the synthesized depth image and on the right a synthesized reflectance image is shown. The synthesized images are overlaid on the real images.

Denoting the Jacobian with

$$A_{ijk}^{(1)} = \left. \frac{\partial f_{ijk}^{(1)}}{\partial \mathbf{p}} \right|_{\mathbf{p}^{(\nu)}} \quad A_{ijk}^{(2)} = \left. \frac{\partial f_{ijk}^{(2)}}{\partial \mathbf{p}} \right|_{\mathbf{p}^{(\nu)}} \quad (12)$$

and

$$\Delta l_{ijk}^{(1)} = \lambda_{ijk}(d_l) - f_{ijk}^{(1)}(\mathbf{p}^{(\nu)}) \quad (13)$$

$$\Delta l_{ijk}^{(2)} = I(\mathbf{x}_{ijk}) - f_{ijk}^{(2)}(\mathbf{p}^{(\nu)}) \quad (14)$$

one obtains the parameter covariance as (cf. (Förstner and Wrobel, 2004), p.87)

$$C_{pp}^{(\nu+1)} = \left(\sum_i^N \sum_j^M \sum_k^K \frac{1}{\sigma_{jk}^2} A_{ijk}^{T(\tau(k))} A_{ijk}^{(\tau(k))} \right)^{-1} \quad (15)$$

where $\tau(k)$ indicates the current camera type. (1=PMD-camera, 2=CCD-camera) The variance factors σ_{jk} are initially set to 1.

From this the parameter update is computed as

$$\Delta \mathbf{p} = C_{pp} \left(\sum_i^N \sum_j^M \sum_k^K \frac{1}{\sigma_{jk}^2} A_{ijk}^{T(\tau(k))} \Delta l_{ijk}^{(\tau(k))} \right) \quad (16)$$

yielding the improved parameter vector

$$\mathbf{p}^{(\nu+1)} = \mathbf{p}^{(\nu)} + \Delta \mathbf{p} \quad (17)$$

The sum of the squared residuals in a depth or reflectance image are given by:

$$\Omega_{jk} = \sum_i^N \|A_{ijk}^{(\tau(k))} \Delta \mathbf{p} - \Delta l_{ijk}^{(\tau(k))}\|^2 \quad (18)$$

so that the variance factors can be updated according to (cf. (Förstner and Wrobel, 2004), p.91)

$$\left(\sigma_{jk}^{(\nu+1)} \right)^2 = \left(\sigma_{jk}^{(\nu)} \right)^2 \frac{\Omega_{jk}}{R_{jk}} \quad (19)$$

with R_{jk} = the redundancy of the observations j, k . Starting with initial variance factors $\sigma_{jk}^{(0)} = 1$ this process should be

iterated until convergence. We chose as convergence criterion, that the update is smaller than 1% of the expected accuracy, i.e. $\Delta p^{-T} C_{pp}^{-1} \Delta p < 0.01$.

4 RESULTS AND DISCUSSION

For the discussion of the calibration results we will rely on the covariance matrix and discuss the accuracy and correlations of the estimated parameters. In our experiments we used a calibration setup consisting of four cameras, three CCD-cameras and one PMD-camera. Two of the CCD-cameras have a resolution of 640×480 pixel whereas the third CCD-camera has a resolution of 1024×768 pixel. The PMD-camera has an opening angle of $22^\circ \times 16^\circ$ and a resolution of 64×48 pixel. We used a checkerboard pattern as a calibration object, printed out at a size of $\approx 1.5m \times \approx 1m$ (black/white square size $145mm \times 145mm$). We incorporated 320 images, 80 per camera, at different positions in front of the checkerboard and at different distances, covering a distance range of 2.5m to 6.5m. Note that for calibration of the depth error it is essential to cover the whole distance area during the calibration process, whereas for the estimation of the internal camera parameters it is essential to use images where the checkerboard covers the whole fov of the camera.

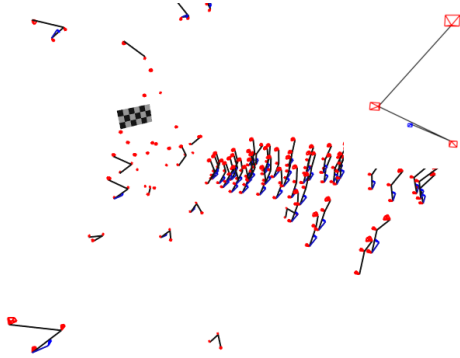


Figure 4: The initial camera positions of all cameras in the rig.

Figure 4 visualizes the initial estimates of the external camera positions relative to the used checkerboard pattern as a result of the methods implemented in (Intel, n.d.). In the top right corner a single camera rig is shown. Recall that the cameras are indexed with $k, k \in (1, \dots, K)$. After the initial parameter estimate the mean relative transformations between camera $k = 0$ and the cameras $k = 1, \dots, K$ are computed. The external camera parameters of camera $k = 0$ and the mean relative parameters of cameras $k = 1, \dots, K$ are optimized in the following.

Figure 5 visualizes the optimized external camera positions relative to the used checkerboard pattern. Again in the top right corner a single camera rig is shown. While the cameras are distributed coarsely in the initial estimate (figure 4), they are properly aligned according to distance after convergence (figure 5).

4.1 Internal Camera Parameters

Tables 1 and 2 show the accuracy of the estimated internal PMD-camera parameters. Focal length and principle point are estimated to sub-pixel accuracy. Note that the used unit *pel* stands for *pixel* as an abbreviation for *P*icture*E*lement.

To interpret the accuracy one has to consider the correlations of internal PMD-parameters. In the tables 3 and 4 the correlations of the internal parameters of the PMD-camera are plotted. It shows that only small correlations are present in the optimized parameter set.

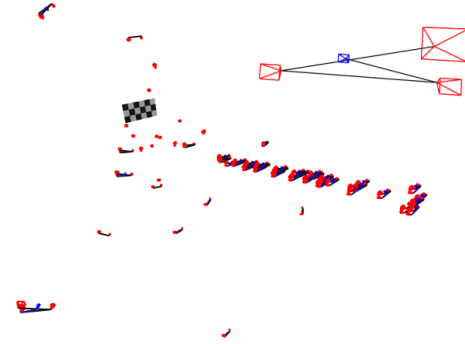


Figure 5: The optimized camera positions of all cameras after calibration.

$\sigma_{f_x} [pel]$	$\sigma_{f_y} [pel]$	$\sigma_{x_H} [pel]$	$\sigma_{y_H} [pel]$	σ_s
0.0059	0.0043	0.0024	0.0022	0.0007

Table 1: Accuracy of the internal PMD-camera parameters. f_x and f_y are the focal lengths in x and y, x_H and y_H is the principle point in x and y and s is the shear.

σ_{r1}	σ_{r2}	σ_{t1}	σ_{t2}
0.0012	0.0040	3.902e-06	1.773e-06

Table 2: Accuracy, r_1 and r_2 are the radial distortion parameters, t_1 and t_2 the tangential distortion parameters.

	$f_x [pel]$	$f_y [pel]$	$x_H [pel]$	$y_H [pel]$	s
$f_x [pel]$	1.000	0.049	-0.103	0.046	-0.093
$f_y [pel]$	0.049	1.000	-0.067	-0.089	-0.017
$x_H [pel]$	-0.103	-0.067	1.000	-0.098	0.027
$y_H [pel]$	0.046	-0.089	-0.098	1.000	0.002
s	-0.093	-0.017	0.027	0.002	1.000
r_1	-0.037	0.039	0.113	0.107	-0.006
r_2	-0.109	-0.246	-0.086	-0.047	-0.024
t_1	0.034	-0.004	-0.047	-0.052	-0.002
t_2	-0.090	0.054	-0.058	-0.101	0.005

Table 3: Correlation of focal length f_x and f_y , principle point x_H and y_H and shear s .

	r_1	r_2	t_1	t_2
$f_x [pel]$	-0.037	-0.109	0.034	-0.090
$f_y [pel]$	0.039	-0.246	-0.004	0.054
$x_H [pel]$	0.113	-0.086	-0.047	-0.058
$y_H [pel]$	0.107	-0.047	-0.052	-0.101
s	-0.006	-0.024	-0.002	0.004
r_1	1.000	-0.271	2.0e-4	-0.037
r_2	-0.271	1.000	-0.016	0.01
t_1	2.0e-4	-0.016	1.000	-0.272
t_2	-0.037	0.01	-0.272	1.000

Table 4: Correlation of radial and tangential distortion parameters.

4.2 External Camera Parameters

In the evaluated calibration setup we used four cameras with 80 images each. To evaluate the accuracy of the external camera parameters we show the mean accuracy of the 80 external camera positions and rotations of the first camera in our camera rig. Note that the position and rotation of the other cameras is estimated relative to this first camera. Table 5 shows the mean accuracy of the 80 external camera parameters.

$\sigma_X [mm]$	$\sigma_Y [mm]$	$\sigma_Z [mm]$	$\sigma_\omega [^\circ]$	$\sigma_\phi [^\circ]$	$\sigma_\kappa [^\circ]$
0.063	0.046	0.271	4.73e-6	4.94e-6	7.91e-6

Table 5: Mean accuracy of all external camera parameters

Standard deviation of the external calibration:

$\sigma_X [mm]$	$\sigma_Y [mm]$	$\sigma_Z [mm]$	$\sigma_\omega [^\circ]$	$\sigma_\phi [^\circ]$	$\sigma_\kappa [^\circ]$
0.006	0.009	0.004	1.38e-7	1.77e-7	1.22e-7

Table 6: Standard deviation of mean accuracy of the external camera parameters

Comparing the results in table 5 to the calibration approach in (Beder and Koch, 2007) where only one PMD-image is used, one can see that the accuracy is significantly improved by the presented method. The accuracy of the camera position is improved by the order of two magnitudes in the direction parallel to the calibration pattern. In the direction orthogonal to the calibration pattern the accuracy is improved by a factor of two. The accuracy of the rotation estimation is significantly improved as well. However note, that these values reflect the mean accuracy of the external parameters of all camera. Observing very small values for the standard deviations in table 6 yields that the average is a good indication for the single cameras.

A well-known problem in camera calibration and computer vision applications is the dependency between intrinsic parameters (focal length) and camera translation and rotation. In (Beder and Koch, 2007) this correlation is examined for the case of calibrating one PMD-camera. Because of the narrow opening angle of about $22^\circ \times 16^\circ$ the correlations between translation and rotation are strong and the real values could not be estimated to satisfaction. In contrast to that the correlation is significantly reduced by the combination of the PMD-camera with (multiple) CCD-cameras. In table 7 the mean correlations of the external camera parameters all show small correlations. Only Z and κ show some correlation as ϕ and X do. However these correlations are by far less than in (Beder and Koch, 2007).

	$X [mm]$	$Y [mm]$	$Z [mm]$	$\omega [^\circ]$	$\phi [^\circ]$	$\kappa [^\circ]$
X	1.000	-0.122	-0.422	0.029	-0.250	-0.074
Y	-0.122	1.000	0.194	0.011	-0.035	-0.058
Z	-0.422	0.194	1.000	-0.079	0.003	-0.004
ω	0.029	0.011	-0.079	1.000	-0.017	-0.175
ϕ	-0.250	-0.035	0.003	-0.017	1.000	-0.075
κ	-0.074	-0.058	-0.004	-0.175	-0.075	1.000

Table 7: Mean correlation of the external camera parameters

	$X [mm]$	$Y [mm]$	$Z [mm]$	$\omega [^\circ]$	$\phi [^\circ]$	$\kappa [^\circ]$
X	0.000	0.127	0.032	0.005	0.015	0.012
Y	0.127	0.000	0.039	0.014	0.004	0.009
Z	0.032	0.039	0.000	0.003	0.005	0.003
ω	0.005	0.014	0.002	0.000	0.013	0.010
ϕ	0.015	0.004	0.005	0.013	0.000	0.008
κ	0.012	0.009	0.003	0.010	0.008	0.000

Table 8: Standard deviation of the mean correlation of the external camera parameters

4.3 Distance Deviation

The distance error is an important issue for applications using PMD-cameras. Some approaches to calibrate and define the distance error function have been proposed (e.g.(Kolb and Lindner, 2006)). However we found our definition in equation 8 to suit the observed distance error, while not over-fitting the calibration data.

$d_0 [mm]$	$d_1 [mm]$	$d_2 [\frac{1}{\text{per}}]$	$d_3 [\frac{1}{\text{per}}]$	$d_4 [\frac{mm}{m^2}]$	$d_5 [\frac{mm}{m^3}]$
-912.922	0.972	0.845	-0.943	-0.0003	2.347e-08

Table 9: The estimated distance parameters

σ_{d_0}	σ_{d_1}	σ_{d_2}	σ_{d_3}	σ_{d_4}	σ_{d_5}
109.918	0.077	0.083	0.113	1.73e-05	1.27e-09

Table 10: Accuracy of the distance parameters

The absolute values of the distance error function are shown in table 9 and the accuracy of the distance error parameters is pictured in table 10.

	d_0	d_1	d_2	d_3	d_4	d_5
d_0	1.000	-0.996	-0.004	0.027	0.987	-0.972
d_1	-0.996	1.000	-0.02	-0.053	-0.997	0.988
d_2	-0.004	-0.02	1.000	-0.024	0.019	-0.018
d_3	0.027	-0.053	-0.024	1.000	0.055	-0.059
d_4	0.987	-0.997	0.019	0.055	1.000	-0.997
d_5	-0.972	0.988	-0.018	-0.059	-0.997	1.000

Table 11: Correlation of the distance parameters.

In table 11 it is visible that the offset d_0 is highly correlated with the inclination d_1 and the higher order terms of the polynomial d_4 and d_5 are highly correlated with d_0 and d_1 .

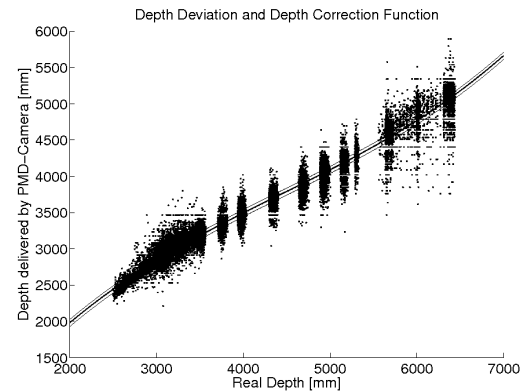


Figure 6: Per pixel depth deviation and correction function.

Figure 6 displays the real depth (x-axis) against the measurement of the PMD-camera (y-axis) per pixel for all used PMD-images. The real depth is computed by estimating the pose of the PMD-camera relative to the calibration pattern using the estimated internal camera parameters. The lines in the graph are the depth calibration function 8 plotted with the estimated parameters from table 9. The thicker line is for the principle points, the small line above and below the thicker line are for $x = 0, y = 0$ and $x = 63, y = 47$. At first glance it is surprising that no offset is visible compared to the values in table 9. But the value of the offset d_0 is compensated by the higher order terms d_1 and d_5 . The graph also shows a high scattering in the depth measurement, especially at distances $> 5.5m$. Although only very few measurements show this high scattering the used camera is obviously not suitable for measurements at distances $> 5.5m$.

Figure 7 shows the mean remaining depth error after calibration with the standard deviations for all used PMD-images. The depth measurement error before calibration is between 100mm and 1.3m, dependent on the distance. The mean remaining error is reduced to $\approx 100mm$ within the full operation range. This is due to the bad SNR as can be seen in figure 2. Apparently the standard deviations are fairly high, especially from 5.5m onwards. The ideal operation distance of this camera is therefore below 5.5m.

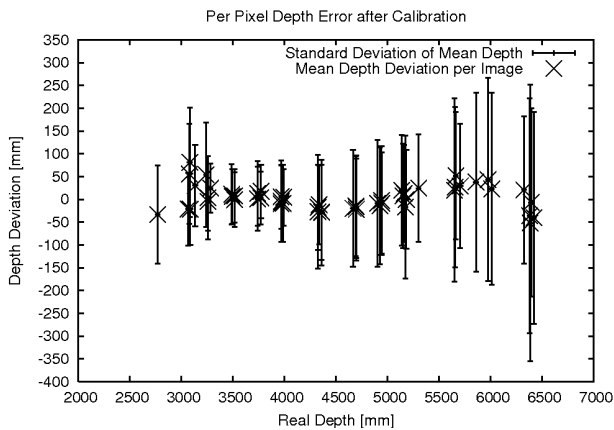


Figure 7: The remaining per pixel depth error after application of the depth error function. The mean errors per image are shown together with their standard deviations.

5 CONCLUSIONS AND FURTHER WORK

We presented a powerful and accurate calibration method for PMD-cameras in combination with multiple standard CCD-cameras. We use standard computer vision algorithms for the initial parameter estimation. Optimization of the parameters is done using an analysis-by-synthesis approach. The used model is a rendered smoothed checkerboard pattern. In contrast to point-based calibration methods we obtain a measurement for every pixel and our method is independent of the used calibration model. The parameters are estimated using non-linear optimization. This method enables us to overcome the limitations of the small opening angle today's PMD-cameras suffer from. Especially the correlations between translation and rotation could be reduced to a satisfying minimum. Additionally the depth error function of the PMD-camera is simultaneously estimated. A remaining positioning error in the component orthogonal to the calibration pattern of the PMD-camera is estimated into the depth calibration parameters. Using the depth error function in combination with the estimated camera matrix this effect will compensate itself.

Based on the observations in this contribution regarding small field-of-view and low SNR, an improved PMD-camera prototype has been developed and will be exploited in the future.

This calibration, especially the combination of standard CCD-cameras and PMD-cameras is especially useful in applications where a combination of such cameras is required. Interesting future work will include the incorporation of fish-eye cameras in the calibration procedure. This requires another camera model but will be very useful for many applications.

ACKNOWLEDGMENTS

This work was supported by the German Research Foundation (DFG) as part of the 3DPoseMap project (KO-2044/3-1).

REFERENCES

Beder, C. and Koch, R., 2007. Calibration of focal length and 3d pose based on the reflectance and depth image of a planar object. In: Proceedings of the Dyn3D Workshop.

Beder, C., Bartzak, B. and Koch, R., 2007a. A Comparison of PMD-Cameras and Stereo-Vision for the Task of Surface Reconstruction using Patchlets. In: IEEE/ISPRS Workshop BenCOS 2007.

Beder, C., Bartzak, B. and Koch, R., 2007b. A combined approach for estimating patchlets from PMD depth images and stereo intensity images. In: F. Hamprecht, C. Schnörr and B. Jähne (eds), Proceedings of the DAGM 2007, LNCS, Springer, pp. 11–20.

Bouguet, J., 1999. Visual methods for three-dimensional modelling. PhD thesis.

Förstner, W. and Wrobel, B., 2004. Mathematical concepts in photogrammetry. In: J.C.McGlone, E.M.Mikhail and J.Bethel (eds), Manual of Photogrammetry, ASPRS, pp. 15–180.

Fuchs, S. and May, S., 2007. Calibration and registration for precise surface reconstruction with tof cameras. In: Proceedings of the DAGM Dyn3D Workshop, Heidelberg, Germany.

Heikkila, J. and Silven, O., 1997. A four-step camera calibration procedure with implicit image correction. In: CVPR '97: Proceedings of the 1997 Conference on Computer Vision and Pattern Recognition (CVPR '97), IEEE Computer Society, Washington, DC, USA, p. 1106.

Intel, n.d. openCV: Open source Computer Vision library. <http://www.intel.com/research/mrl/research/opencv/>.

Kahlmann, T., Remondino, F. and Ingensand, H., 2006. Calibration for increased accuracy of the range imaging camera Swiss-rangerTM. In: IEVM06.

Kolb, A. and Lindner, M., 2006. Lateral and depth calibration of pmd-distance sensors. In: International Symposium on Visual Computing (ISVC06).

Kraft, H., Frey, J., Moeller, T., Albrecht, M., Grothof, M., Schink, B., Hess, H. and Buxbaum, B., 2004. 3d-camera of high 3d-frame rate, depth-resolution and background light elimination based on improved pmd (photonic mixer device)-technologies. In: 6th International Conference for Optical Technologies, Optical Sensors and Measuring Techniques (OPTO 2004).

Kuhnert, K. and Stommel, M., 2006. Fusion of stereo-camera and PMD-camera data for real-time suited precise 3d environment reconstruction. In: IEEE/RSJ International Conference on Intelligent Robots and Systems (IROS).

Lange, R., Seitz, P., Biber, A. and Schwarte, R., 1999. Time-of-flight range imaging with a custom solid-state imagesensor. In: EOS/SPIE Laser Metrology and Inspection, Vol. 3823.

Lindner, M. and Kolb, A., 2006. Lateral and depth calibration of PMD-distance sensors. In: International Symposium on Visual Computing (ISVC06), Vol. 2, Springer, pp. 524–533.

Mugnier, C. J., Förstner, W., Wrobel, B., Paderes, F. and Munjy, R., 2004. The mathematics of photogrammetry. In: J.C.McGlone, E.M.Mikhail and J.Bethel (eds), Manual of Photogrammetry, ASPRS, pp. 181–316.

Prasad, T., Hartmann, K., Wolfgang, W., Ghobadi, S. and Sluiter, A., 2006. First steps in enhancing 3d vision technique using 2d/3d sensors. In: V. Chum, O.Franc (ed.), Computer Vision Winter Workshop 2006, Czech Society for Cybernetics and Informatics, University of Siegen, pp. 82–86.

Prusak, A., Melnychuk, O., Schiller, I., Roth, H. and Koch, R., 2007. Pose estimation and map building with a pmd-camera for robot navigation. In: Proceedings of the DAGM Dyn3D Workshop, Heidelberg, Germany.

Streckel, B., Bartzak, B., Koch, R. and Kolb, A., 2007. Supporting structure from motion with a 3d-range-camera. In: Scandinavian Conference on Image Analysis (SCIA07).

Xu, Z., Schwarte, R., Heinol, H., Buxbaum, B. and Ringbeck, T., 1998. Smart pixel - photonic mixer device (pmd). In: M2VIP 98 - International Conference on Mechatronics and Machine Vision in Practice, pp. 259 – 264.

Zhang, Z., 1999. Flexible Camera Calibration by Viewing a Plane from Unknown Orientations. In: Proceedings of the International Conference on Computer Vision, Corfu, Greece, pp. 666–673.